CVI Journals.ASM.org

Needle-Free Dermal Delivery of a Diphtheria Toxin CRM_{197} Mutant on Potassium-Doped Hydroxyapatite Microparticles

Nikolas T. Weissmueller,[a,b,c] Heiko A. Schiffter,[b] Robert C. Carlisle,[b] Christine S. Rollier,[a,c] Andrew J. Pollard[a,c]

Oxford Vaccine Group, Department of Pediatrics, University of Oxford, and NIHR Oxford Biomedical Research Institute, Oxford, United Kingdom[a]; Biomedical Ultrasonics, Biotherapy & Biopharmaceuticals Laboratory, University of Oxford, Oxford, United Kingdom[b]; The Oxford Martin School, University of Oxford, Old Indian Institute, Oxford, United Kingdom[c]

Injections with a hypodermic needle and syringe (HNS) are the current standard of care globally, but the use of needles is not without limitation. While a plethora of needle-free injection devices exist, vaccine reformulation is costly and presents a barrier to their widespread clinical application. To provide a simple, needle-free, and broad-spectrum protein antigen delivery platform, we developed novel potassium-doped hydroxyapatite (K-Hap) microparticles with improved protein loading capabilities that can provide sustained local antigen presentation and release. K-Hap showed increased protein adsorption over regular hydroxyapatite ($P < 0.001$), good structural retention of the model antigen (CRM_{197}) with 1% decrease in α-helix content and no change in β-sheet content upon adsorption, and sustained release *in vitro*. Needle-free intradermal powder inoculation with K-Hap–CRM_{197} induced significantly higher IgG1 geometric mean titers (GMTs) than IgG2a GMTs in a BALB/c mouse model ($P < 0.001$) and induced IgG titer levels that were not different from the current clinical standard ($P > 0.05$), namely, alum-adsorbed CRM_{197} by intramuscular (i.m.) delivery. The presented results suggest that K-Hap microparticles may be used as a novel needle-free delivery vehicle for some protein antigens.

The number of immunizations rises annually with population growth, vaccine availability, and sophistication of immunization schedules. Consequently, the risk associated with needles as a vector of infection is contributing to the global burden of disease (1–3). Of the 16 billion therapeutic injections administered with needles and syringes in 2004 globally, 800 million were prophylactic inoculations, and approximately 30 million of the 16 billion (or 0.19%) resulted in needlestick injuries, some of which have transmitted blood-borne pathogens, such as HIV, hepatitis B, or hepatitis C (4, 5).

While a plethora of needle-free inoculation devices exists, most needle-free immunization technologies require the reformulation of vaccines that are routinely administered with a hypodermic needle and syringe (HNS) (6–8). In the case of protein antigens, dry-powder manufacture for intradermal or mucosal delivery is largely empirical and hence particularly costly, which presents a barrier to the widespread use of needle-free inoculation (9–13).

Protein antigens are often poorly immunogenic and generally require the addition of an adjuvant to elicit robust antibody responses (14, 15). Colloidal adjuvants, such as aluminum salts, are routinely used to boost vaccine immunogenicity (16). However, previous efforts to reformulate vaccines for use in needle-free intradermal injection have linked aluminum salt coformulation with an increased aggregate content and the denaturation of the protein antigen after lyophilization or spray lyophilization (17–21). Furthermore, alum has been reported to induce granuloma formation when injected intradermally (22). While alum adjuvantation is problematic in combination with lyophilization and dermal inoculation, a novel dermal delivery vehicle may not require alum adjuvantation.

The potential use of calcium phosphate-based scaffolds as a drug delivery vehicle has been extensively researched and is well documented (23, 24). In particular, hydroxyapatite (Hap), a biocompatible mineral that is naturally found in bone and largely comprises of calcium and phosphate, has been shown to strongly adsorb proteins and to provide sustained release of the bioactive molecule (25, 26). Recently, it was reported that a commercial calcium phosphate adjuvant consisted of nanosized Hap needles (27). Therefore, Hap has demonstrated its capability to act as a drug and vaccine delivery substrate and has a documented track record of biocompatibility and safety and may potentiate the immune response to antigens.

Here, we investigate whether intradermal delivery of Hap microparticles can elicit antibody titers to the adsorbed CRM_{197} protein antigen, using the Venturi needle-free ballistic injection device (28). The diphtheria toxin mutant CRM_{197} protein is a 58-kDa, two-subunit, nontoxic protein that is frequently used as a polysaccharide carrier protein in commercial glycoconjugate vaccines, but it is poorly immunogenic without adjuvantation (29–31). To our knowledge, this is the first report of needle-free ballistic intradermal immunization with CRM_{197} using Hap microparticles.

MATERIALS AND METHODS

K-Hap particle manufacture. Potassium-substituted hydroxyapatite (K-Hap) microparticles were manufactured by molten salt synthesis. The protocol was adapted from the method of Viswanath et al. (32). Briefly,

Received 3 March 2015 **Accepted** 21 March 2015

Accepted manuscript posted online 25 March 2015

Citation Weissmueller NT, Schiffter HA, Carlisle RC, Rollier CS, Pollard AJ. 2015. Needle-free dermal delivery of a diphtheria toxin CRM_{197} mutant on potassium-doped hydroxyapatite microparticles. Clin Vaccine Immunol 22:586–592. doi:10.1128/CVI.00121-15.

Editor: M. F. Pasetti

Address correspondence to Nikolas T. Weissmueller, nikolas.weissmueller@gmail.com.

doi:10.1128/CVI.00121-15

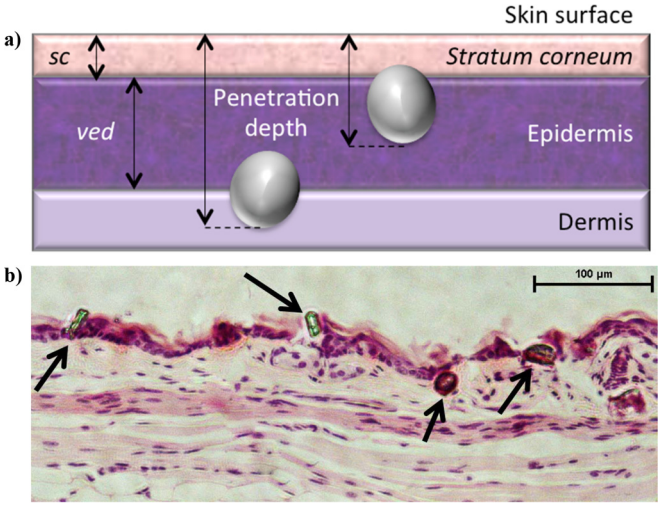

FIG 1 (a) The thickness of the stratum corneum (SC) and viable epidermis (VED) were measured as depicted by the two-headed arrows. The particle penetration depth was measured as the length of the line that connects the deepest part of a particle in the tissue to the outer part of the stratum corneum and is perpendicular to the latter. The distances in pixels were related to the microscope's calibration scale to obtain distance measurements in micrometers. (b) Microscopy slides of hematoxylin-and-eosin (H&E)-stained tissue sections were imaged with a Nikon Eclipse T*i* light microscope, and the penetration depths of K-Hap particles (arrows) were measured and analyzed using ImageJ.

pure Hap powder (Sigma-Aldrich, Dorset, United Kingdom) was ball milled with potassium sulfate salt (Sigma-Aldrich, Dorset, United Kingdom) at a 1:6 ratio by weight. The blended powders were sintered in a high-alumina crucible (Sigma-Aldrich, Dorset, United Kingdom) at 1,200°C for 3.5 h and cooled to room temperature at 5°C/min. Excess salt was removed with hot deionized water.

Injection depth and dermal measurements. Female BALB/c mice (6 to 8 weeks old) were purchased from Harlan. All animals were maintained under appropriate conditions at the Functional Genomics Facility at Oxford University, United Kingdom, and animal procedures were performed in accordance with the terms of the United Kingdom Home Office Animals Act Project License. Procedures were approved by the University of Oxford Animal Care and Ethical Review Committee. The fur was clipped and shaved on the abdomen and at the base of the tail. Injection sites were prepped with 70% ethanol prior to injection. Hap microparticles were injected at a gas pressure of 55×10^5 Pa using the in-line Venturi needle-free powder injection device (Particle Therapeutics Ltd., Yarton, United Kingdom). Histology samples from the injection sites were fixed in 10% buffered formalin, dehydrated in alcohol, embedded in paraffin wax, sectioned every 5 μm, and stained with hematoxylin and eosin (Sigma-Aldrich, Dorset, United Kingdom). Images were obtained on a Nikon Eclipse T*i* light microscope with NIS Elements AR 3.0 software. The particle penetration depth and the viable epidermis (VED) and stratum corneum (SC) thicknesses were assessed using ImageJ analysis software (available at http://rsb.info.nih.gov/ij; developed by Wayne Rasband, National Institutes of Health, Bethesda, MD, USA). The particle injection depth was measured based on the microscope's calibrated size scale, and it was reported as the distance between the outer part of the SC and the location on the particle furthest in the tissue (Fig. 1a and b). The localization of particles in the epidermis was determined by comparing the mean particle penetration depth to the location of the VED-to-dermis threshold, which was defined as the mean SC-plus-VED thickness at a given injection location. Because the diameter of K-Hap particles is larger than the SC thickness, if their penetration depth is similar or less than the SC-plus-VED threshold, particles are located at least partially in the epidermis.

Hap and K-Hap BSA-TRITC loading. Hap and K-Hap 10-mg powder samples were incubated at room temperature (RT) for 3 h with 5 mg of bovine serum albumin (BSA)-tetramethyl rhodamine isothiocyanate (TRITC) (Sigma-Aldrich, Dorset, United Kingdom) in 1 ml of phosphate-buffered saline (PBS) (Sigma-Aldrich, Dorset, United Kingdom) at pH 7.4 on a VWR rotating shaker (VWR, Dublin, Ireland). Protein loading on Hap and K-Hap was determined by micro-bicinchoninic acid (micro-BCA) assay kit according to the manufacturer's recommendations (Sigma-Aldrich, Dorset, United Kingdom). In addition to the bulk average protein loading measured by BCA assay, the protein loading on individual particles was characterized using fluorescence imaging. Briefly, protein loading of albumin-TRITC on dry-powder Hap and K-Hap was assessed using fluorescence imaging at 80-ms exposure and ×4 magnification on a Nikon Eclipse T*i* light microscope and NIS Elements AR 3.0 software. Albumin-TRITC was excited at 550 nm, and fluorescence was monitored at 600 nm. Fluorescence intensity was averaged over the respective particle area using ImageJ analysis software and reported from low to high on an 8-bit (0 to 255) gray-scale intensity spectrum.

K-Hap CRM_{197} dry-powder formulation. The model antigen CRM_{197} (Novartis Vaccines and Diagnostics, Siena, Italy) was provided in 10% (wt/vol) sucrose–10 mM K_2HPO_4 at pH 7.2 and was dialyzed against PBS (pH 7.4) for 12 h using a Mini Slide-A-Lyzer (Fisher Scientific, Loughborough, United Kingdom) with a 10-kDa-molecular-size cutoff prior to use. Dialyzed CRM_{197} was adsorbed onto 10 mg of K-Hap particles in 1 ml of PBS (pH 7.4) for 3 h at 1.6 mg/ml on a VWR rotating shaker. The slurry was centrifuged for 3 min at 2,000 × *g* (MSE, London, United Kingdom), and the supernatant was subsequently decanted. The K-Hap–CRM_{197} particles were washed thrice with isopropanol (Fisher Scientific, Loughborough, United Kingdom). The wet powder was then transferred into lyophilization vials (Adelphi Healthcare Packaging, Haywards, United Kingdom) and vacuum dried for 24 h at 13.33 Pa and 20°C with a FTS Lyostar I instrument (SP Industries, Warminster, PA, USA). The vials were sealed, crimped, and stored at room temperature until further use.

K-Hap CRM_{197} adsorption and *in vitro* release. The total protein loading on K-Hap (C_0) was determined as the percentage of the mass difference between CRM_{197} in solution before and after adsorption measured by micro-BCA assay (Sigma-Aldrich, Dorset, United Kingdom) and divided by the mass of K-Hap. The Langmuir isotherm is described by the following equation:

$$y = (abx^{1-c})/(1 + bx^{1-c})$$

and was iteratively fitted using GraphPad Prism 5 (GraphPad Software, Inc., San Diego, CA, USA). The dependent variable y (in milligrams per gram) is the amount of CRM_{197} per mass of K-Hap, the independent variable x (in milligrams per liter) is the CRM_{197} concentration in solution. The variable a is the adsorption capacity, while b and c are model constants. The approximate surface area of particles was obtained on a Malvern Mastersizer S analyzer (Malvern Instruments Ltd., Malvern, United Kingdom), in a small-volume dispersion cell. A 300RF lens with backscatter detector with an active beam length of 14.3 mm was used to obtain an average of 6 times 6,000 measurements according to Mie theory. Particles were added until 10 to 13% detector obscuration was achieved at a stirring rate of 2,000 rpm. Refractive indices (RI) for HA and K-Hap particles (RI, 1.6510) dispersed in deionized (dI) water (RI, 1.3300) were used in the method.

CRM_{197} release from K-Hap in PBS was quantified by micro-BCA assay (Sigma-Aldrich, Dorset, United Kingdom) after 0, 0.5, 1.5, 6, and 24 h of incubation in PBS (pH 7.4) at 37°C on a rotating shaker ($n = 3$). Absorbance at 562 nm was measured on a Cary 50 Bio UV-visible spectrophotometer (Varian, CA, USA). Concentrations were plotted as percent release relative to total protein loading (C/C_0).

Structural characterization of surface-adsorbed CRM_{197}. The secondary structure of CRM_{197} when adsorbed on K-Hap or aluminum phosphate (Adju-Phos; Brenntag Biosector, Frederikssund, Denmark) was determined using a LN_2-cooled Fourier transform infrared (FT-IR) Tensor 37 spectrometer, equipped with the attenuated total reflection

BioATR II sample compartment (Bruker Optics, Ettlingen, Germany). Over the range 4,000 to 800 cm^{-1}, 128 scans were averaged at a 4-cm^{-1} resolution. The attenuated total reflection (ATR) unit was temperature controlled at 20°C. OPUS 6.5 software data postprocessing included atmospheric compensation, vector normalization, baseline correction, and integration of the amide I and II band regions from 1,720 cm^{-1} to 1,480 cm^{-1}. The spectra were evaluated against the Quant II structural database provided by Bruker Optics.

Immunization. Six- to 8-week-old female BALB/c mice (Harlan, Oxfordshire, United Kingdom) were fully anesthetized with isoflurane gas. Before needle-free administration of K-Hap–CRM_{197}, the murine pinna was sterilized with 70% ethanol solution. The in-line Venturi device (Particle Therapeutics Ltd., Yarnton, United Kingdom) was placed onto the dorsal pinna for injection. Medical-grade helium pressured at 55×10^5 Pa was used to accelerate the K-Hap powder containing 10 μg CRM_{197} into the skin. Intramuscular injection with 12.5 μl of aqueous CRM_{197} was administered into the medial thigh of each hind leg using a 29-gauge needle. The total volume of 25 μl contained 10 μg CRM_{197}, with or without alum ($n = 8$). Briefly, CRM_{197} was formulated with Adju-Phos at a ratio of 10 μg CRM_{197} to 85 μg alum in 10 mM Tris buffer (pH 7.0 to 7.5). For 10 doses, 30 μl of saline was added to 170 μl of Adju-Phos containing 850 μg of aluminum under aseptic conditions. After 15 min at room temperature, 50 μl of a 2-mg/ml CRM_{197} solution was added and incubated at room temperature for 1 h prior to injection. Naive mice served as a negative control ($n = 4$). Mice were primed on day 0 and boosted on day 28 with the same formulations and antigen dose. Blood was collected from the tail vein on days 28 and 42.

ELISA. Antibody responses were assessed by enzyme-linked immunosorbent assay (ELISA) after coating plates (Fisher Scientific, Loughborough, United Kingdom) with 5 μg of CRM_{197} antigen per well in carbonate-bicarbonate buffer (Sigma-Aldrich, Dorset, United Kingdom). The reactions in the wells were blocked with PBS containing 5% BSA (Sigma-Aldrich, Dorset, United Kingdom). Serum samples were serially diluted in PBS containing 0.05% Tween 20 (PBS–Tween) with 5% BSA at a starting dilution of 1:200. After incubation at 25°C for 2 h, an antibody detecting goat anti-mouse antibody (Southern Biotech, Cambridge, United Kingdom) was added at a dilution of 1:2,000 in PBS–Tween with 5% BSA. After 1-h incubation of the plates, the reactions in the wells were developed with 3,3′,5,5′-tetramethylbenzidine substrate (Sigma-Aldrich, Dorset, United Kingdom) for 10 min and stopped with 2 M sulfuric acid (Sigma-Aldrich, Dorset, United Kingdom). The optical density at 405 nm (OD_{405}) was read with a Multiskan EX microplate reader (Thermo Scientific, Loughborough, United Kingdom). Results were expressed as endpoint titers where the reciprocal of the highest serum dilution gives a reading above the cutoff value. The cutoff value was established as the OD_{405} of the sample diluent plus 2 standard deviations.

Statistics. Statistical methods included unpaired two-tailed Student *t* test, one-way analysis of variance (ANOVA) with Tukey-Kramer multiple comparison correction, and two-way ANOVA with Bonferroni posttest for multiple comparison correction. The alpha level of 0.05 was considered to be statistically significant. The statistical analysis was performed and graphically displayed using GraphPad Prism 5 (GraphPad Software, Inc., San Diego, CA, USA).

RESULTS

Intradermal particle placement by location. An initial dermal particle penetration study was conducted to determine the injection location that achieved preferential targeting of the epidermis. For this, histology samples were taken from the injection sites on the ear, abdomen, and base of tail (BoT) after needle-free injection to assess the thickness of the dermal layers and the penetration depth of the Hap microparticles by microscopy (Fig. 1a and b). One-way ANOVA results on histology measurements suggest that the thickness of the viable epidermis (VED) varied significantly ($P < 0.001$) between inoculation locations. The greatest mean thickness was observed for the pinna (36.3 μm), while the mean VED thickness for the abdomen and BoT ranged between 20.1 and 22.5 μm (Table 1). The stratum corneum (SC) had significantly different thicknesses ($P < 0.001$) at the various injection sites. Also, the mean particle penetration depth (MPD) was significantly different ($P < 0.01$) for the three injection sites. The MPD was not different for the abdomen and BoT ($P > 0.05$). Colocalization of particles with the epidermis is best when the MPD approximates the SC-plus-VED thickness (Fig. 1a). The best colocalization of Hap particles within the viable epidermis was observed for pinna injections with a MPD of 53.7 μm ± 19.2 μm and SC-plus-VED thickness of 52.5 μm ± 14.0 μm (Table 1). MPD exceeded the SC-plus-VED threshold at both of the other injection sites. Therefore, the dry-powder vaccine was injected needle-free into the pinna in the subsequent immunogenicity study.

TABLE 1 Microscopy measurements on histology samples describing powder placement in the skin and dermal dimensions[a]

Sample location	Viable epidermal thickness (μm)	Stratum corneum thickness (μm)	Particle penetration depth (μm)
Pinna	36.3 ± 8.1 (135)	16.2 ± 5.9 (148)	53.7 ± 19.2 (69)
Abdomen	22.5 ± 5.2 (162)	6.6 ± 2.7 (161)	46.3 ± 19.2 (195)
Base of tail	20.1 ± 9.8 (157)	9.9 ± 5.5 (187)	44.4 ± 19.0 (178)

[a] Values are reported as means ± standard deviations (SD). The number of observations is shown in parentheses.

Protein adsorption onto Hap and K-Hap. An increased surface adsorption propensity can increase the antigen payload that is delivered per microparticle and thereby reduce the extraneous material delivered per dose. Using fluorescence microscopy, it was determined that the mean adsorption of albumin-TRITC in physiological PBS was significantly greater ($P < 0.001$) on K-Hap than on Hap (Fig. 2b). These results were confirmed by micro-BCA assay (data not shown). Fluorescence images suggested some variability in protein loading within the Hap and K-Hap particle groups (Fig. 2a). This may be attributable to variation in particle surface properties such as surface roughness, material composition, and surface charge of individual particles. Although particle morphology varied between prismic and spheroidal, there was no apparent effect of morphology on protein adsorption.

Secondary structure of surface-adsorbed CRM_{197}. Immunogenic epitopes may be adversely affected by changes in the secondary structure of the antigen, which should be avoided during dry-powder formulation. FT-IR analysis of surface-adsorbed CRM_{197} suggested that the amide I band peak position of K-Hap-adsorbed CRM_{197} was observed at 1,648 cm^{-1} (Table 2). This was also the amide I band peak position of CRM_{197} when CRM_{197} was suspended in phosphate buffer. Adsorption onto K-Hap caused a 1% reduction in α-helix content but no detectable increase in β-sheet content relative to the solution. This suggests that adsorption onto K-Hap largely conserved the native secondary structure of CRM_{197}. On the other hand, alum-adsorbed CRM_{197} induced a 5% decrease of α-helical content along with a 5% increase in β-sheet structures (Table 2). These results suggest that a form of CRM_{197} that is more similar to the native state may be presented to the immune system on K-Hap than on alum.

CRM_{197} adsorption isotherm on K-Hap. The surface sorption capacity of CRM_{197} on K-Hap was determined as a function of protein concentration in the suspension based on the measured

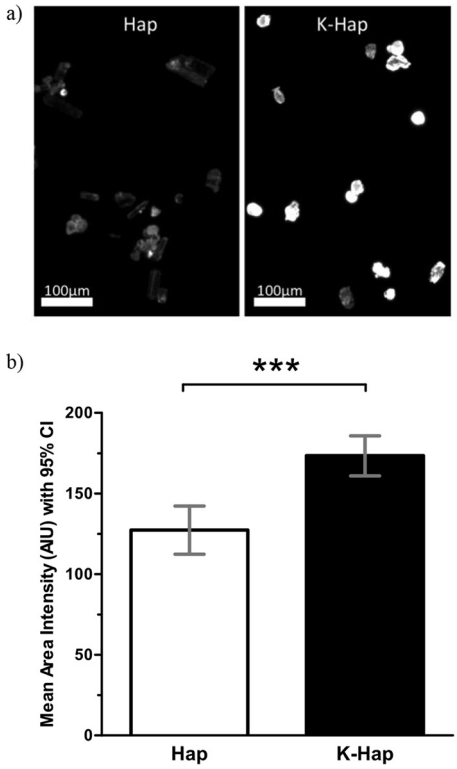

FIG 2 (a and b) Albumin-TRITC (5 mg/ml) was adsorbed onto 10 mg Hap and K-Hap in PBS (pH 7.4) for 3 h on a rotating shaker, then washed thrice with isopropanol, and vacuum dried at 13.33 Pa for 24 h at 20°C. Dry-Hap–albumin–TRITC and K-Hap–albumin–TRITC powders were imaged at 80-ms exposure under ×4 magnification. Fluorescence of albumin-TRITC was excited at 550 nm and monitored at 600 nm. (b) Emission intensity values were quantified as mean area intensity with 95% confidence interval (95% CI) and averaged over the visible individual particle area using 8-bit gray-scale values (0 to 255) in ImageJ. A total of 90 particles were studied. Values that are significantly different ($P < 0.001$) by an unpaired two-tailed t test at $\alpha = 0.05$ significance level are indicated (***).

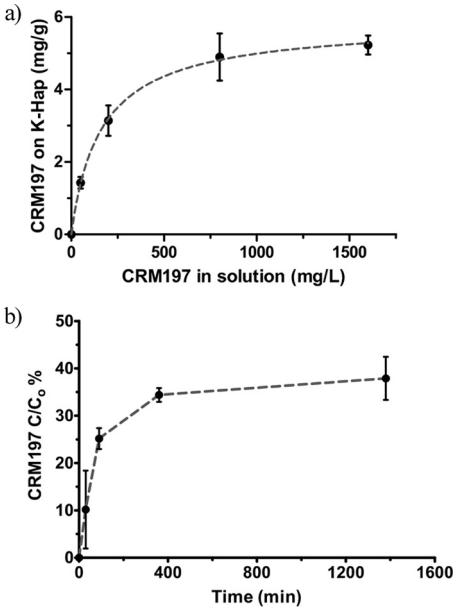

FIG 3 CRM_{197} adsorption and release from K-Hap *in vitro*. (a) CRM_{197} sorption onto K-Hap in 10 mM PBS (pH 7.4) at room temperature for 3 h as a function of protein concentration in solution. Changes in the CRM_{197} concentration in PBS were measured using a micro-BCA assay. Mean adsorbed CRM_{197} mass with standard deviation plotted relative to K-Hap follows a Langmuir isotherm ($R^2 = 0.988$; $n = 3$; repeated 3 times). (b) Mean cumulative release and standard deviation ($n = 3$; repeated 3 times) of CRM_{197} in PBS (pH 7.4) from K-Hap microparticles were measured using a micro-BCA assay. The cumulative release (C) is expressed relative to the total adsorbed protein on the K-Hap microparticles (C_0) over time.

mass of CRM_{197} per mass of K-Hap. Figure 3a suggests that CRM_{197} adsorption on K-Hap is well described by the Langmuir isotherm ($R^2 = 0.988$). Computational extrapolation estimates the adsorption capacity at 5.9 mg of CRM_{197} per g of K-Hap as the maximum amount of CRM_{197} per gram of substrate. When related to the particle surface area obtained from the light-scattering particle size distribution, the maximum CRM_{197} adsorption capacity corresponds to a surface protein loading density on K-Hap of 9.7 mg/m^2.

Time-dependent CRM_{197} release. Colloidal adjuvants retain the antigen at the injection site, which has been linked to immune response potentiation. K-Hap microparticles released approximately 28% of their maximum 5.9 mg of CRM_{197} per g of K-Hap payload within the first 90 min in PBS buffer as an initial burst but provided sustained release of the antigen thereafter (Fig. 3b). Therefore, K-Hap may similarly retain CRM_{197} at the injection site, like aluminum adjuvants, while providing a slow release of the antigen.

TABLE 2 Secondary structure of CRM_{197} measured by total attenuated reflection FT-IR[a]

CRM_{197} form	Substrate	α-Helix content (%)	β-Sheet content (%)	Amide I peak position (cm^{-1})
Adsorbed	K-Hap	30 ± 1	28 ± 1	1,648 ± 0.5
	Alum	26 ± 1	33 ± 1	1,648 ± 0.5
In solution	PBS	31 ± 0.5	28 ± 0.5	1,648 ± 0.1

[a] Values are reported as means ± SD ($n = 3$).

Serum IgG antibody response. Pathogen opsonization, agglutination, and toxin neutralization are facilitated by the presence of IgG in serum. It was investigated whether K-Hap–CRM_{197} could induce IgG levels similar to that of the current clinical standard (e.g., alum-CRM_{197}). As depicted in Fig. 4a, anti-CRM_{197} serum IgG geometric mean titers (GMTs) were not different for alum-adsorbed CRM_{197} and K-Hap-adsorbed CRM_{197} 28 days after prime ($P > 0.05$), although the mean IgG GMT for K-Hap-adsorbed CRM_{197} was higher on average. On day 42, 14 days after the booster dose, alum-adsorbed CRM_{197} GMTs were higher on average than in the K-Hap-adsorbed CRM_{197} group, but the difference was not significant ($P > 0.05$). Both alum and K-Hap conditions showed significantly higher mean GMTs than the naive control ($P < 0.001$). An approximately 1.4-fold increase in IgG GMT levels was observed for K-Hap–CRM_{197}, and a 1.7-fold increase in the alum-adjuvanted CRM_{197} condition was seen between days 28 and 42. A nonsignificant trend suggests that K-Hap may induce a stronger initial response than alum-CRM_{197} (administered intramuscularly [i.m.]), but alum-adsorbed CRM_{197} may have a stronger booster response.

IgG subclass responses. It was investigated whether the pre-

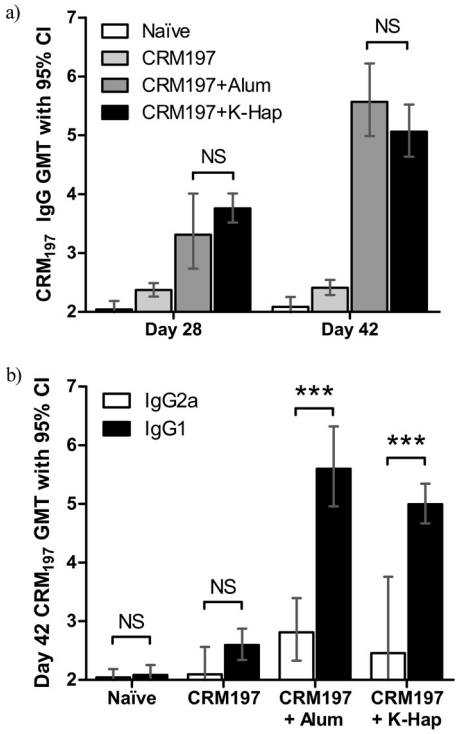

FIG 4 All treatment groups ($n = 8$) received 10 μg CRM_{197} on days 0 (prime) and 28 (boost). Mice were bled on days 28 and 42. Naive mice served as the control group (four mice). Preimmunization serial titers were less than 200. CRM_{197} alone in PBS (CRM197) and CRM_{197} adjuvanted with 85 μg alum (CRM197+Alum) were injected i.m. with HNS. K-Hap–CRM_{197} powder was administered intradermally (i.d.) needle-free (CRM197+K-Hap). (a) The IgG geometric mean titer (GMT) and 95% confidence interval (95% CI) are indicated for all treatment groups on days 28 and 42. (b) IgG1 and IgG2a GMTs with 95% CIs are indicated for all treatment groups on day 42. Two-way ANOVA compared the categorical variables (a) "treatment group" and "time point" and (b) "treatment group" and "IgG subclass" as predictors of the continuous-variable CRM_{197} GMT and was conducted at $\alpha = 0.05$ significance level. Values that are significantly different ($P < 0.001$) are indicated (***). *P* values above the α-level were considered not significant (NS).

sentation of CRM_{197} in the K-Hap microparticle surface-adsorbed state could influence the IgG1/IgG2a balance. The alum-adjuvanted and needle-free K-Hap groups both showed a 2-fold IgG1/IgG2a-biased response. These results suggest that alum and K-Hap may similarly act as adjuvant and induce an IgG1-biased response. Two weeks after the booster dose (day 42), anti-CRM_{197} IgG1 GMTs were higher for the alum-adjuvanted group than for the needle-free K-Hap group ($P < 0.05$). Both the alum-adjuvanted and K-Hap-adjuvanted ($P < 0.001$) groups induced significantly higher GMTs than the naive control. These results suggest that K-Hap-adsorbed CRM_{197} injected needle-free induces a similarly IgG1-biased response as alum-adsorbed CRM_{197} by HNS and that K-Hap may act in a similarly adjuvanting manner as alum.

DISCUSSION

While needle-free immunization has clear advantages over inoculation with HNS, the latter is less technically demanding (6). The three pivotal aspects of successful needle-free intradermal vaccination are the antigen payload deposition in the correct dermal layer, the structural preservation of the antigen during dry-powder formulation, and the magnitude and type of immune response that can be elicited compared to HNS inoculation (33). This paper addresses these three aspects. The data presented show successful targeting of the needle-free vaccine to the epidermis, structural retention of the CRM_{197} protein in the K-Hap-adsorbed state, and comparable immunogenicity of the needle-free delivery approach with CRM_{197}-adsorbed K-Hap relative to the alum-adjuvanted condition by HNS.

Needle-free powder delivery to the optimal dermal layer reportedly presents a challenge in part due to highly variable skin characteristics (34, 35). Previous ballistic delivery studies have emphasized the influence of VED and SC thickness on particle penetration depth, with an increase in layer thickness translating to reduced penetration into the skin (36). In this study, we did not observe this effect on K-Hap penetration depth. A possible reason for this may be the varied K-Hap particle shape factor (spheroidal to prismic) that could influence penetration properties or the relatively large particle size relative to the dermal layers. However, the thicker SC and VED layers in the pinna allowed for good colocalization of K-Hap particles with the epidermis, whereas particles penetrated too deep at the other injection sites. Interestingly, while differences in VED and SC thickness are also thought to impact the particle distribution in the dermis, the obtained results show an almost identical variance about the mean despite significantly different VED and SC dimensions (Table 1). This suggests that while VED and SC thickness can impact the powder penetration depth, they may contribute less to the particle distribution in the skin than other factors, such as the underlying particle characteristics, the injection device, and the propulsion pressure.

An alternative antigen delivery platform should preserve the structure of the antigen and have sufficient antigen-carrying capacity to minimize the codelivery of extraneous material. On solid particles, the antigen-carrying capacity is restricted to surface adsorption. Protein sorption propensity on surfaces is affected by the net surface charge and the distribution of local charges (37). We found that potassium-doped Hap adsorbed significantly more BSA-TRITC than pure Hap did. It is possible that the incorporation of potassium into the Hap crystal lattice may have impacted the material's net surface charge and allowed for an improved protein-loading capacity of the negatively charged BSA-TRITC (Fig. 2a and b). Alternatively, the ionic sorbent properties of K-Hap may be enhanced relative to Hap, and thus may bind a broader set of positively and negatively charged pockets on the protein, as the net overall charge may not adequately account for the presence of charged pockets. Since the protein adsorption on K-Hap was independent of the individual particle morphology, this suggests that the greater adsorption propensity relative to pure Hap is due to a material characteristic rather than to a morphological characteristic (38).

In addition to increased protein loading, K-Hap also largely preserved the secondary structure of CRM_{197}. Partial unfolding of proteins can lead to aggregation via the association of exposed hydrophobic patches to form an intermolecular β-sheet. This change is manifested by a decrease in α-helix structure and an increase in β-sheet content (39). Since CRM_{197} α-helix and β-sheet structures were reasonably well preserved on the K-Hap surface, hydrophobic patches are likely not exposed (Table 2). Therefore, protein aggregation is unlikely to occur even if adsorbed molecules are in sufficiently close physical proximity to interact. The maximum sorption capacity was estimated at 5.9 mg

of CRM_{197} per g of K-Hap and was well-described by a Langmuir isotherm ($R^2 = 0.988$). This suggests that CRM_{197} adsorbed onto K-Hap as a single layer, which correlates with the minor changes in secondary structure observed by FT-IR. When related to the particle surface area, which was obtained from the light-scattering particle size distribution, the maximum CRM_{197} adsorption capacity corresponds to a K-Hap surface protein-loading density of 9.7 mg/m^2. The protein-loading density of BSA on pure hydroxyapatite has been reported as 1.5 mg/m^2, but buffer strength, protein type, and substrate can affect the loading density and may therefore not be compared directly to the results presented in this paper (40). Additionally, light scattering can give an estimate of the surface area, but it cannot account for the surface roughness. Therefore, the average surface loading density of CRM_{197} on K-Hap can be regarded only as a rough estimate. The cumulative CRM_{197} release from the K-Hap particles after 24 h was less than 40% of the total payload, which is less than 2.4 μg of CRM_{197} per 1 mg of K-Hap. Therefore, the possible soluble aggregate content of this formulation can be considered minimal at any given time *in situ* and hence does not pose a serious concern (41, 42). Furthermore, the strong antigen retention on K-Hap suggests a similar antigen depot function as alum, and therefore, K-Hap may be considered an adjuvant, more so than either an immune modulator or an inactive formulation excipient. This theory is supported by the elicited IgG and IgG subclass GMTs.

The magnitude and quality of the induced immune response can provide insight into the effect of a novel antigen formulation (43). In this study, needle-free immunization with K-Hap–CRM_{197} induced geometric mean IgG antibody titers (IgG GMT) that were not different ($P > 0.05$) from alum-adjuvanted CRM_{197} by HNS 4 weeks after prime and 2 weeks after boost. The GMT ratios of IgG1/IgG2a were approximately 2-fold IgG1 biased for the alum-adjuvanted CRM_{197} and K-Hap-adsorbed CRM_{197} groups. Based on the observed IgG and IgG subclass responses, the immune activation with K-Hap-adsorbed CRM_{197} resembled the adjuvant effect observed with alum. The adjuvanticity of alum is partially ascribed to the formation of an antigen depot, as well as to the noncovalently bound surface presentation of the antigen. Based on the physical characterizations of CRM_{197} sorption and release from K-Hap, the adjuvant effect of K-Hap on CRM_{197} immunogenicity may be achieved in a fashion similar to that of aluminum salts.

While immunization with CRM_{197} alone is not of direct clinical applicability, the use of the CRM_{197} protein in this study presents a good model to probe the capability of the K-Hap formulation approach. For example, *Haemophilus influenzae* type b (Hib), pneumococcal, and meningococcal vaccines contain oligosaccharides that are covalently linked to CRM_{197} (30). From a formulation standpoint, the structural preservation of CRM_{197} is the most challenging component of a dry-powder K-Hap vaccine, as it is the protein that likely denatures (44). *In vivo* and FT-IR results suggest that the structure of CRM_{197} was sufficiently preserved. This finding motivates the investigation of the K-Hap platform as a needle-free delivery vehicle for a variety of CRM-based conjugate vaccines.

In conclusion, the data presented suggest that needle-free intradermal vaccination with CRM_{197} antigen-loaded K-Hap microparticles induces an IgG1-biased antibody response with strong IgG GMTs that are not different from the alum-adjuvanted CRM_{197} by HNS. Simple coincubation of the antigen with the K-Hap carrier microparticles followed by vacuum desiccation was sufficient to reformulate the antigen, whereas conventional pharmaceutical dry-powder formulation processes require the need for largely empirical excipient selection and time-consuming spray lyophilization, which can degrade proteins. In the surface-adsorbed state, CRM_{197} largely retained its secondary structure according to FT-IR measurements. These findings encourage the investigation of the *in vivo* immunogenicity of needle-free glycoconjugate formulations using the K-Hap vehicle.

ACKNOWLEDGMENTS

We thank Novartis Vaccines and Diagnostics for providing the CRM_{197} free of charge, Particle Therapeutics Ltd. for providing the injection device and helium cylinders free of charge, and The Oxford Martin School, Department of Pediatrics and the Biomedical Ultrasonics, Biotherapy & Biopharmaceuticals Laboratory at the University of Oxford for the generous funding.

REFERENCES

1. **Varmus H, Klausner R, Zerhouni E, Acharya T, Daar AS, Singer PA.** 2003. Grand challenges in global health. Science **302:**398–399. http://dx.doi.org/10.1126/science.1091769.
2. **Guo YL, Shiao J, Chuang YC, Huang KY.** 1999. Needlestick and sharps injuries among health-care workers in Taiwan. Epidemiol Infect **122:**259–265. http://dx.doi.org/10.1017/S0950268899002186.
3. **Rapiti E, Prüss-Üstün A, Hutin Y.** 2005. Sharps injuries: assessing the burden of disease from sharps injuries to health-care workers at national and local levels. World Health Organization, Geneva, Switzerland.
4. **Hopkins C.** 2012. Needlestick injuries. Nurs Stand **27**(3):59.
5. **World Health Organization.** 2004. Safety of injections: global facts and figures. World Health Organization, Geneva, Switzerland.
6. **Mitragotri S.** 2005. Immunization without needles. Nat Rev Immunol **5:**905–916. http://dx.doi.org/10.1038/nri1728.
7. **Sullivan SP, Koutsonanos DG, Del Pilar Martin M, Lee JW, Zarnitsyn V, Choi SO, Murthy N, Compans RW, Skountzou I, Prausnitz MR.** 2010. Dissolving polymer microneedle patches for influenza vaccination. Nat Med **16:**915–920. http://dx.doi.org/10.1038/nm.2182.
8. **Prausnitz MR, Langer R.** 2008. Transdermal drug delivery. Nat Biotechnol **26:**1261–1268. http://dx.doi.org/10.1038/nbt.1504.
9. **Fang WJ, Qi W, Kinzell J, Prestrelski S, Carpenter JF.** 2012. Effects of excipients on the chemical and physical stability of glucagon during freeze-drying and storage in dried formulations. Pharm Res **29:**3278–3291. http://dx.doi.org/10.1007/s11095-012-0820-7.
10. **Wang W.** 2000. Lyophilization and development of solid protein pharmaceuticals. Int J Pharm **203:**1–60. http://dx.doi.org/10.1016/S0378-5173(00)00423-3.
11. **Wang W.** 2005. Protein aggregation and its inhibition in biopharmaceutics. Int J Pharm **289:**1–30. http://dx.doi.org/10.1016/j.ijpharm.2004.11.014.
12. **Kersten G, Hirschberg H.** 2007. Needle-free vaccine delivery. Expert Opin Drug Deliv **4:**459–474. http://dx.doi.org/10.1517/17425247.4.5.459.
13. **Weissmueller NT, Schiffter HA, Pollard AJ.** 2013. Intradermal powder immunization with protein-containing vaccines. Expert Rev Vaccines **12:**687–702. http://dx.doi.org/10.1586/erv.13.48.
14. **Snape MD, Perrett KP, Ford KJ, John TM, Pace D, Yu LM, Langley JM, McNeil S, Dull PM, Ceddia F, Anemona A, Halperin SA, Dobson S, Pollard AJ.** 2008. Immunogenicity of a tetravalent meningococcal glycoconjugate vaccine in infants: a randomized controlled trial. JAMA **299:**173–184. http://dx.doi.org/10.1001/jama.2007.29-c.
15. **Pollard AJ, Perrett KP, Beverley PC.** 2009. Maintaining protection against invasive bacteria with protein-polysaccharide conjugate vaccines. Nat Rev Immunol **9:**213–220. http://dx.doi.org/10.1038/nri2494.
16. **Lindblad EB.** 2004. Aluminium compounds for use in vaccines. Immunol Cell Biol **82:**497–505. http://dx.doi.org/10.1111/j.0818-9641.2004.01286.x.
17. **Chen D, Erickson CA, Endres RL, Periwal SB, Chu Q, Shu C, Maa YF, Payne LG.** 2001. Adjuvantation of epidermal powder immunization. Vaccine **19:**2908–2917. http://dx.doi.org/10.1016/S0264-410X(00)00544-2.
18. **Chen DX, Kristensen D.** 2009. Opportunities and challenges of developing thermostable vaccines. Expert Rev Vaccines **8:**547–557. http://dx.doi.org/10.1586/erv.09.20.

19. **Maa YF, Ameri M, Shu C, Payne LG, Chen D.** 2004. Influenza vaccine powder formulation development: spray-freeze-drying and stability evaluation. J Pharm Sci **93:**1912–1923. http://dx.doi.org/10.1002/jps.20104.
20. **Maa YF, Shu C, Ameri M, Zuleger C, Che J, Osorio JE, Payne LG, Chen D.** 2003. Optimization of an alum-adsorbed vaccine powder formulation for epidermal powder immunization. Pharm Res **20:**969–977. http://dx.doi.org/10.1023/A:1024493719236.
21. **Maa YF, Ameri M, Shu C, Zuleger CL, Che J, Osorio JE, Payne LG, Chen D.** 2007. Hepatitis-b surface antigen (hbsag) powder formulation: process and stability assessment. Curr Drug Deliv **4:**57–67. http://dx.doi.org/10.2174/156720107779314758.
22. **Marsee DK, Williams JM, Velazquez EF.** 2008. Aluminum granuloma after administration of the quadrivalent human papillomavirus vaccine. Report of a case. Am J Dermatopathol **30:**622–624. http://dx.doi.org/10.1097/DAD.0b013e318185a691.
23. **Verron E, Khairoun I, Guicheux J, Bouler JM.** 2010. Calcium phosphate biomaterials as bone drug delivery systems: a review. Drug Discov Today **15:**547–552. http://dx.doi.org/10.1016/j.drudis.2010.05.003.
24. **Ginebra MP, Canal C, Espanol M, Pastorino D, Montufar EB.** 2012. Calcium phosphate cements as drug delivery materials. Adv Drug Deliv Rev **64:**1090–1110. http://dx.doi.org/10.1016/j.addr.2012.01.008.
25. **Yin G, Liu Z, Zhan J, Ding FX, Yuan NJ.** 2002. Impacts of the surface charge property on protein adsorption on hydroxyapatite. Chem Eng J **87:**181–186. http://dx.doi.org/10.1016/S1385-8947(01)00248-0.
26. **Shen JW, Wu T, Wang Q, Pan HH.** 2008. Molecular simulation of protein adsorption and desorption on hydroxyapatite surfaces. Biomaterials **29:**513–532. http://dx.doi.org/10.1016/j.biomaterials.2007.10.016.
27. **Jiang DP, Premachandra GS, Johnston C, Hem SL.** 2004. Structure and adsorption properties of commercial calcium phosphate adjuvant. Vaccine **23:**693–698. http://dx.doi.org/10.1016/j.vaccine.2004.06.029.
28. **Costigan G, Liu Y, Brown GL, Carter FV, Bellhouse BJ.** 2005. Evolution of the design of Venturi devices for the delivery of dry particles to skin or mucosal tissue, p 719–724 . *In* Jiang Z (ed), Shock waves. Proceedings of the 24th International Symposium on Shock Waves, Beijing, China, 11 to 16 July 2004. Springer-Verlag, Berlin, Germany.
29. **Malito E, Bursulaya B, Chen CN, Lo Surdo P, Picchianti M, Balducci E, Biancucci M, Brock A, Berti F, Bottomley MJ, Nissum M, Costantino P, Rappuoli R, Spraggon G.** 2012. Structural basis for lack of toxicity of the diphtheria toxin mutant CRM197. Proc Natl Acad Sci U S A **109:**5229–5234. http://dx.doi.org/10.1073/pnas.1201964109.
30. **Shinefield HR.** 2010. Overview of the development and current use of crm197 conjugate vaccines for pediatric use. Vaccine **28:**4335–4339. http://dx.doi.org/10.1016/j.vaccine.2010.04.072.
31. **Kanra G, Viviani S, Yurdakok K, Ozmert E, Anemona A, Yalcin S, Demiralp O, Bilgili N, Kara A, Cengiz AB, Mutlu B, Baldini A, Marchetti E, Podda A.** 2003. Effect of aluminum adjuvants on safety and immunogenicity of Haemophilus influenzae type b-crm197 conjugate vaccine. Pediatr Int **45:**314–318. http://dx.doi.org/10.1046/j.1442-200X.2003.01706.x.
32. **Viswanath B, Raghavan R, Gurao NP, Ramamurty U, Ravishankar N.** 2008. Mechanical properties of tricalcium phosphate single crystals grown by molten salt synthesis. Acta Biomater **4:**1448–1454. http://dx.doi.org/10.1016/j.actbio.2008.02.031.
33. **Dean HJ, Fuller D, Osorio JE.** 2003. Powder and particle-mediated approaches for delivery of DNA and protein vaccines into the epidermis. Comp Immunol Microbiol Infect Dis **26:**373–388. http://dx.doi.org/10.1016/S0147-9571(03)00021-3.
34. **Kendall M, Mitchell T, Wrighton-Smith P.** 2004. Intradermal ballistic delivery of micro-particles into excised human skin for pharmaceutical applications. J Biomech **37:**1733–1741. http://dx.doi.org/10.1016/j.jbiomech.2004.01.032.
35. **Kendall M, Rishworth S, Carter F, Mitchell T.** 2004. Effects of relative humidity and ambient temperature on the ballistic delivery of microparticles to excised porcine skin. J Investig Dermatol **122:**739–746. http://dx.doi.org/10.1111/j.0022-202X.2004.22320.x.
36. **Kendall MAF, Chong Y-F, Cock A.** 2007. The mechanical properties of the skin epidermis in relation to targeted gene and drug delivery. Biomaterials **28:**4968–4977. http://dx.doi.org/10.1016/j.biomaterials.2007.08.006.
37. **Hartvig RA, van de Weert M, Ostergaard J, Jorgensen L, Jensen H.** 2011. Protein adsorption at charged surfaces: the role of electrostatic interactions and interfacial charge regulation. Langmuir **27:**2634–2643. http://dx.doi.org/10.1021/la104720n.
38. **Weissmueller NT, Schiffter HA, Pollard AJ, Cuneyt TA.** 2014. Molten salt synthesis of potassium-containing hydroxyapatite microparticles used as protein substrate. Mater Lett **128:**421–424. http://dx.doi.org/10.1016/j.matlet.2014.04.154.
39. **Fink AL.** 1998. Protein aggregation: folding aggregates, inclusion bodies and amyloid. Fold Des **3:**R9–R23. http://dx.doi.org/10.1016/S1359-0278(98)00002-9.
40. **Mavropoulos E, Costa AM, Costa LT, Achete CA, Mello A, Granjeiro JM, Rossi AM.** 2011. Adsorption and bioactivity studies of albumin onto hydroxyapatite surface. Colloids Surf B Biointerfaces **83:**1–9. http://dx.doi.org/10.1016/j.colsurfb.2010.10.025.
41. **den Engelsman J, Garidel P, Smulders R, Koll H, Smith B, Bassarab S, Seidl A, Hainzl O, Jiskoot W.** 2011. Strategies for the assessment of protein aggregates in pharmaceutical biotech product development. Pharm Res **28:**920–933. http://dx.doi.org/10.1007/s11095-010-0297-1.
42. **Rosenberg AS.** 2006. Effects of protein aggregates: an immunologic perspective. AAPS J **8:**E501–E507. http://dx.doi.org/10.1208/aapsj080359.
43. **Plotkin SA.** 2010. Correlates of protection induced by vaccination. Clin Vaccine Immunol **17:**1055–1065. http://dx.doi.org/10.1128/CVI.00131-10.
44. **Peters GH, van Aalten DM, Edholm O, Toxvaerd S, Bywater R.** 1996. Dynamics of proteins in different solvent systems: analysis of essential motion in lipases. Biophys J **71:**2245–2255. http://dx.doi.org/10.1016/S0006-3495(96)79428-6.